

14

Recent Advances in Imaging of Male Reproductive Tract Malignancies

Jurgen J. Fütterer¹, MD PhD and J. Roan Spermon², MD PhD

Key Points

- Testicular ultrasound is the initial investigative tool with regard to scrotal masses.
- Testicular cancer has a five-year survival rate exceeding 95 percent.
- Ninety-five percent of all testicular tumors are germ cell tumors.
- The sensitivity of testicular ultrasound in detecting testicular tumors is almost 100 percent.
- Computed tomography is used for staging metastatic disease and for follow-up after therapy in patients with disseminated disease.
- Positron emission tomography and MRI adds little to the management of clinical stage I non-seminoma germ cell cancer.

1 Introduction

The male reproductive system includes those organs whose function is to accomplish reproduction. This consists of testes, which produce spermatozoa and hormones, a series of ducts that store and transport the sperm, seminal vesicles, the prostate and the penis.

Cancer of the male reproductive system includes testicular, prostatic and penile neoplasms. Testicular cancer is the most common cancer in men between 15- to 35-years-old, and about 36,000 men are diagnosed with testicular cancer each year. Prostate cancer is the most frequently diagnosed malignancy in males. Cancer of

¹Departments of Radiology

²Departments of Urology

^{1,2}Radboud University Nijmegen Medical Centre, Geert Grooteplein zuid 10, NL 6500 HB, Nijmegen, The Netherlands

Corresponding author:

Jurgen J. Fütterer (J.Futterer@rad.umcn.nl)

the penis is rare in western males, but more common in South East Asia and India. It is most often diagnosed in men over the age of 60 years. This chapter will present an overview of imaging of male reproductive tract malignancies.

2 Prostate Cancer

Prostate cancer is the most frequently diagnosed malignancy in western males and the incidence is increasing [1]. It is predicted that in 2007 in the United States alone 218,890 men will be diagnosed with prostate cancer [1]. This is partly due to a growing population of elderly man, but a major factor is the expanding use of the prostate-specific antigen (PSA) test as a prostate cancer biomarker. Between 1989 and 2002, the age-standardized incidence rate of prostate cancer increased by 21.3 percent in the United States. However, at the same time epidemiological surveys demonstrated decreased prostate cancer mortality in several countries since 1993. This decrease in mortality is mostly attributed to earlier diagnosis with a reduction in the number of men with distant metastases. From autopsy studies it is known that prostate cancer can be found in 55 percent of men in their fifth decade and 64 percent in their seventh decade, respectively [2-4]. Prostate cancer is very common in elderly males, and it occurs with a lifetime risk of one in 10 [1]. However, only one in eight of these men will die from this disease [1].

All patient and tumor characteristics must be evaluated to determine the treatment that optimally suits the individual patient. Most often, PSA level, the results of digital rectal examination and histopathological biopsy findings are used for this purpose. However, imaging plays an important role to detect, localize and to stage prostate cancer. This directly influences the diagnostic work-up and may lead to important changes in treatment strategy.

2.1 Prostate Anatomy

On the basis of its embryological origins the prostate is anatomically divided into three zones that are eccentrically located around the urethra: the innermost transition zone, the central zone and the outermost peripheral zone [5, 6]. In older patients the former two cannot be distinguished radiologically due to compression of the central zone by benign prostatic hyperplasia (BPH) in the transitional zone; therefore they are collectively referred to as the central gland, as opposed to the outer gland, which is composed of the peripheral zone. The prostate is divided into the apex and the base. The latter is directed upward and is applied to the inferior surface of the bladder. The apex is directed downward and is in contact with the superior fascia of the urogenital diaphragm.

There is still a debate about whether the prostate has a capsule or not. The prostate is surrounded by a thick layer of fibromuscular tissue corresponding to the capsule. The 'true' prostatic capsule, however, is a thin (0.5 to 2 mm) layer of connective tissue located externally to the peripheral zone. Around this layer there is a

pelvic fascia, often called the “false” prostatic capsule. Satter, et al. considered the prostate capsule as an extension of the prostate parenchyma itself [7, 8].

The periprostatic venous plexus surrounds the gland and drains into the internal iliac veins and the presacral veins. The neurovascular bundles course along the posterolateral aspect of the gland and is a preferential path for tumor spread due to small nerve branches penetrating the prostate capsule in this area.

Knowledge of the zonal anatomy of the prostate is useful considering that many prostatic diseases have a zonal distribution. More than 70 percent of adenocarcinoma of the prostate arises in the peripheral zone, whereas about 20 percent emerge in the transitional zone and 10 percent in the central zone.

2.2 Detection and Localization of Prostate Cancer

In its early stage prostate cancer is commonly asymptomatic because most cancers are located in the peripheral zone. A few patients have symptoms of the lower urinary tract due to obstruction. Prostate cancer patients rarely present with symptoms of haematuria or haematospermia. Prostate cancer is suspected in patients with elevated PSA values.

The urologic work-up in patients with elevated PSA consists of a digital rectal examination and transrectal ultrasound (TRUS). The positive predictive value of a digital rectal examination in the detection of prostate cancer depends on the patient’s age, race, and serum PSA value. In a screening population the positive predictive value varies from 4 percent to 11 percent (PSA 0 to 2.9 ng/mL), and from 33 percent to 83 percent (PSA > 3 ng/mL) [9, 10]. The reproducibility and the inter-observer agreement of a digital rectal examination are limited [11, 12].

2.3 Transrectal Ultrasound (TRUS)

Grayscale TRUS appearance of prostate cancer is a hypoechoic lesion in the peripheral zone. Other conditions such as prostatitis and prostatic intraepithelial neoplasia may also present as hypoechoic lesions (Fig. 14.1) [13, 14]. It is important to note that over 40 percent of prostate cancer lesions are isoechoic while only 5 percent are hyperechoic [15]. The positive predictive value of the hypoechoic lesion in the average urologic population ranged from 18 percent to 53 percent [16]. The systematic TRUS-guided biopsy protocol (sample tissue at standard locations) has become the most common biopsy technique [17]. The number of cores taken per session varies across institutions. Prostate cancer detection rates have varied from 19 percent to 40 percent [18, 19] and repeat biopsy sessions are often necessary [20].

Color Doppler TRUS – Doppler imaging enables the detection of blood flow to or from the ultrasound probe. Increased blood flow due to neovascularity is one of the characteristics of prostate cancer. Doppler enhancement correlated with the microvessel density and Gleason score of a lesion in a study of 96 patients with lower urinary tract symptoms, and PSA levels over 4 ng/ml [21]. Prostate cancer detection rates up to 40 percent were detected using Doppler TRUS [22]. Doppler

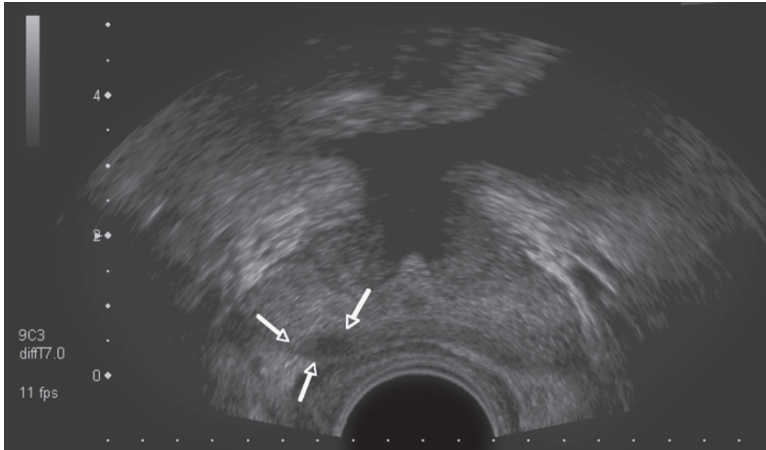


Fig. 14.1 Axial gray-scale transrectal ultrasound image of the prostate of a 55-year-old man (PSA level, 5.7 ng/mL, Gleason sum score, 7 and normal digital rectal examination). A hypo-echoic lesion was observed in the right peripheral zone (arrows)

TRUS imaging resulted in a high inter-observer variability [23, 24] and wide variation in sensitivity and specificity of 27 percent to 92 percent and 46 percent to 84 percent, respectively.

Contrast-enhanced TRUS – A new development is the application of gas-filled microbubble contrast agents (Fig. 14.2.). The microbubbles remain intravascular and, thus, act as blood pool agents. Disadvantages of using contrast agents are the longer duration and higher degree of invasiveness of the examination: however, the risk of hypersensitivity to the substance is rare. Contrast agent-specific imaging techniques have been developed to optimize microbubble signal reception while preserving the microbubbles. Until now, three studies directly compared systematic and contrast-enhanced-targeted TRUS biopsy [25-27]. These studies showed significantly higher positive biopsy core rates when directing biopsy, based on focal areas of contrast enhancement. Sensitivities and specificities of prostate cancer detection using contrast agents varied between 48 percent to 94 percent and 46 percent to 88 percent, respectively.

Sonoelastography – A novel ultrasound technique that analyzes the compressional characteristics of prostate tissue is transrectal sonoelastography. In a recent study of 404 men undergoing biopsy based on real-time sonoelastography revealed a detection rate of 37.4 percent [28]. A drawback of the study was the heterogeneity of the population since more than half of the patients had already undergone one or more negative biopsy sessions. A study comparing real-time elastography with radical prostatectomy reported a localization sensitivity of 88 percent [29].

2.4 Computed Tomography (CT)

A study by Prado and Wallace revealed that contrast-enhanced CT scanning was able to detect only 58 percent of the 102 histologic prostate cancer sites documented

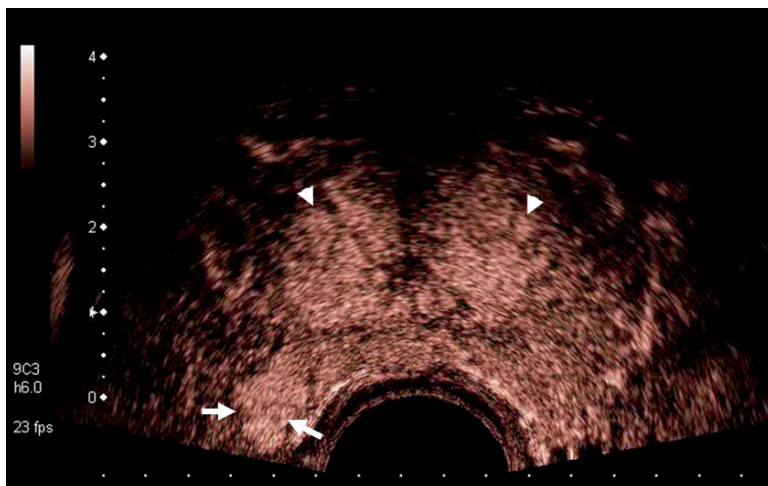


Fig. 14.2 Contrast-enhanced transrectal ultrasound image in contrast-harmonic mode. After a 2.4ml bolus injection of microbubble contrast agent an area of enhancement in the right lateral peripheral zone (arrows) was visible and showed marked enhancement, compared with the rest of the peripheral zone. A symmetrical enhancement of the central gland (arrowheads) was observed

by TRUS-guided biopsies in 25 patients [30]. CT scanning has too little soft tissue contrast resolution to discern the subtle tissue changes due to prostate cancer. CT should not be used for prostate cancer detection and localization.

2.5 Magnetic Resonance Imaging (MRI)

Anatomical MRI – MRI of the prostate is performed using a combination of an endorectal and pelvic phased array coils. On T2-weighted MR images, in the peripheral zone normal prostate tissue appears as an intermediate to high signal intensity, while the central gland has lower signal intensity than the peripheral zone (Fig. 14.3.). Conversely, the prostate has a homogeneous, intermediate signal intensity on T1-weighted images. This means differentiation between the peripheral zone and central gland cannot be perceived.

On MRI prostate cancer appears as an area of low signal intensity within the brighter, healthy peripheral zone using a T2-weighted sequence (Fig. 14.4.). In the central gland, prostate cancer is not as clearly discernable because the central gland generally has lower signal intensity than the peripheral zone, and it is more inhomogeneous due to BPH-induced architectural changes that may mimic prostate cancer. In addition to carcinoma, the differential diagnosis of an area of low signal intensity includes post-biopsy hemorrhage, prostatitis, BPH, effects of hormone or radiation treatment, scars, calcifications, smooth muscle hyperplasia and fibromuscular hyperplasia

MRI plays no role as a screening imaging modality in patients with suspected prostate cancer. In patients with a prior negative TRUS-guided biopsy, T2-weighted

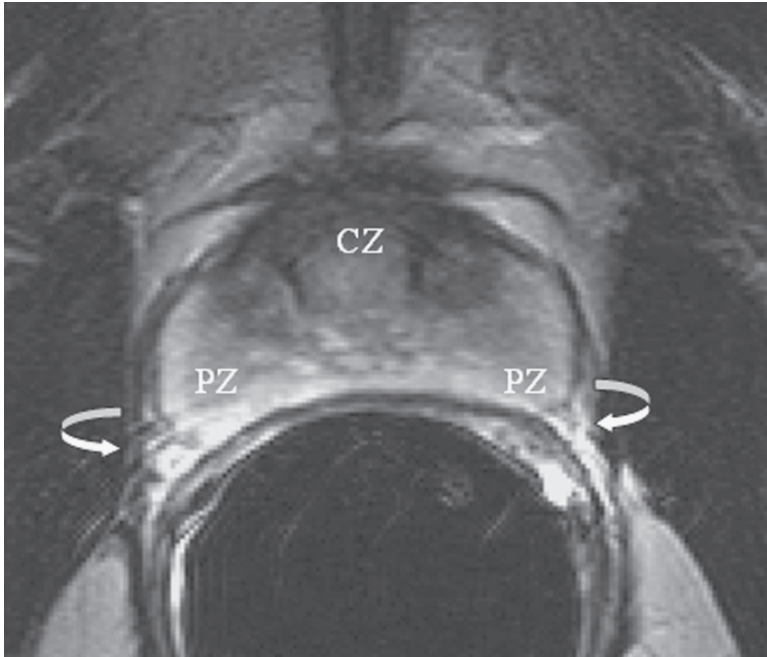


Fig. 14.3 Normal prostate in a 28-year-old man. T2-weighted MRI image shows peripheral zone (PZ) with intermediate to high signal intensity. Small central gland (CG) has lower signal intensity than does the peripheral zone. The neurovascular bundle is located at the posterolateral aspect of the gland (curved arrow)

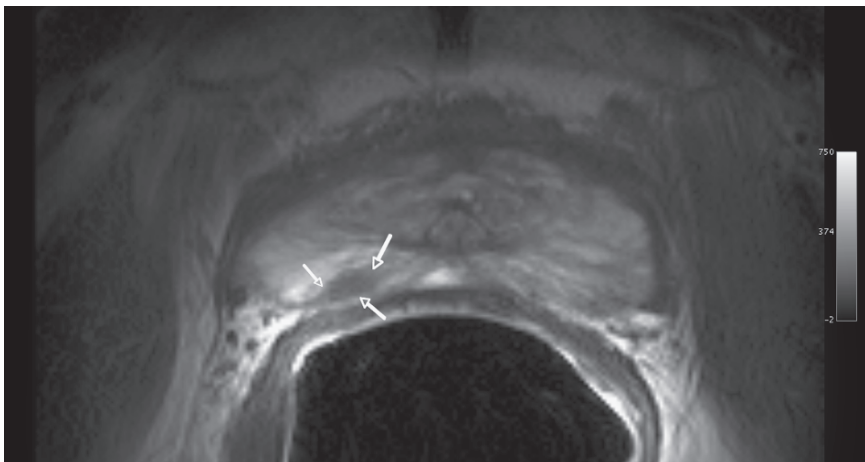


Fig. 14.4 55-year-old man (same patient as in Fig. 14.1) with stage T2a prostate cancer in the right peripheral zone. The T2-weighted MRI image shows that the tumor (*arrows*) has a lower signal intensity compared with the rest of the peripheral zone

MRI plays an important role. In this patient population an 83 percent sensitivity and a 50 percent positive predictive value for MRI have been established [31].

Proton MR spectroscopic imaging (MRSI) – provides quantitative metabolic data based on the citrate, choline and creatine levels, as well as their ratios. MRSI can be used for detection and localization of prostate cancer (Fig. 14.5) [32, 33]. The addition of MRSI to MRI increased the localization accuracy of MRI, particularly by raising specificity up to 91 percent [34]. However, a limitation of MRSI is its

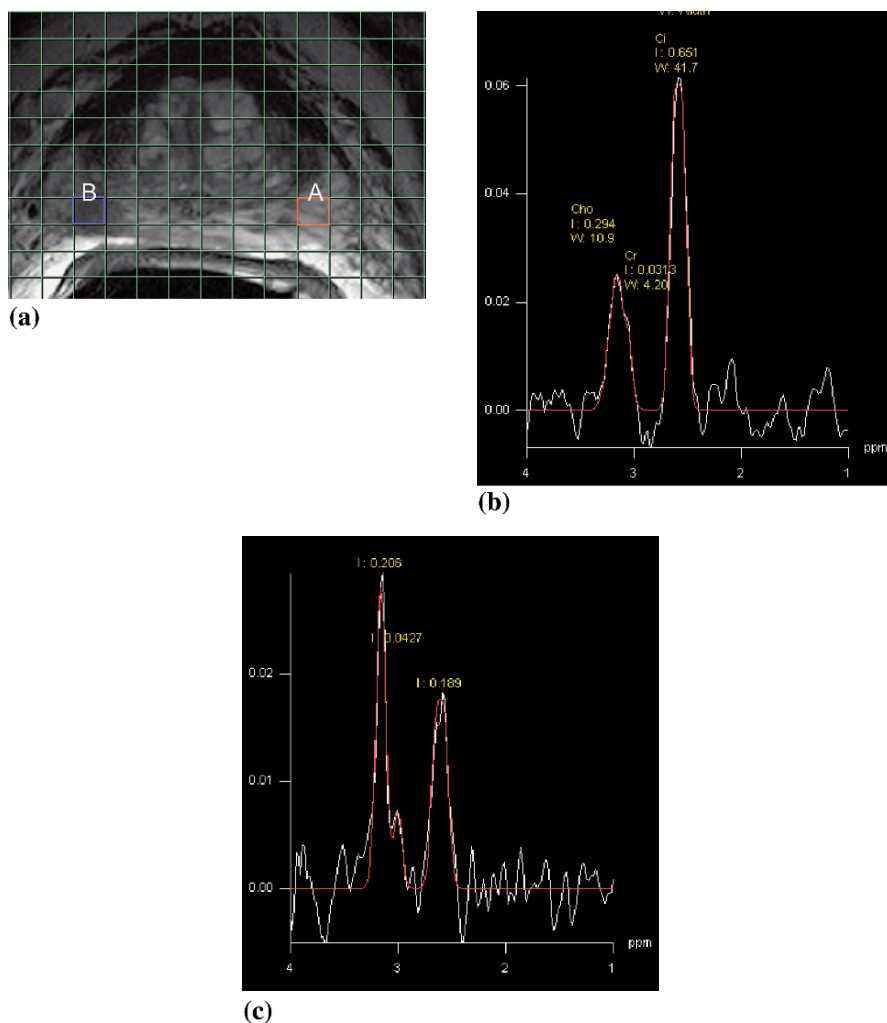


Fig. 14.5 In (a), the position of the voxel of which spectrum (b) and (c) originate from is indicated. The axial T2-weighted image of this patient shows a low signal intensity in the right peripheral zone which is suspicious for prostate cancer. MRI spectra (b) from a voxel in healthy left peripheral zone (high level of citrate and normal low level of choline and creatine) and from a voxel (c) that contained prostate cancer (decreased level of citrate and increased level of choline and creatine)

low spatial resolution. MRSI significantly increased the area under the receiver operating curve, from 0.68 with regular anatomical MRI to 0.80 [35].

Dynamic contrast-enhanced MRI (DCE-MRI) – DCE-MRI is a technique in which the contrast agent concentration is followed in time [36]. This technique is reported to be an effective tool in visualizing the pharmacokinetics of gadolinium uptake in the prostate [37–39]. Early contrast enhancement and high (relative) peak enhancement are the most accurate predictors of prostate cancer of the peripheral zone, while washout of the contrast agent and high permeability of the blood vessels are most sensitive for central gland prostate cancer [40, 41]. A recent study showed that the area under the receiver operating curve for localizing prostate cancer increased significantly, from 0.68 with anatomical T2-weighted MRI, to 0.91 by applying contrast agent (Fig. 14.6) [35].

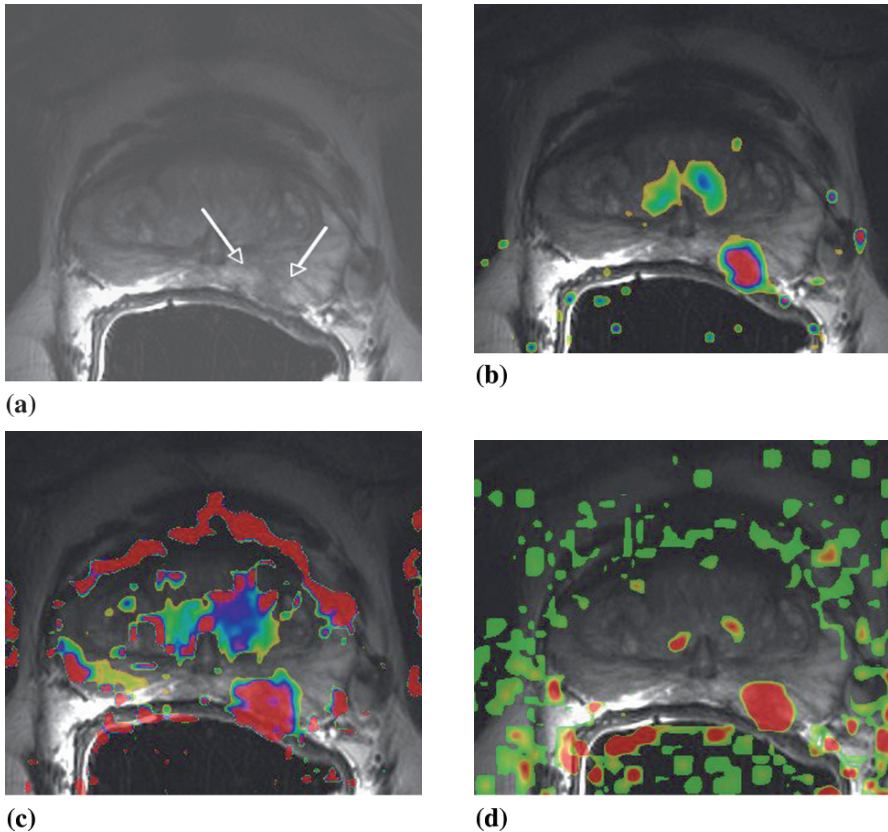


Fig. 14.6 MR images of the prostate of 65-year-old man with prostate cancer (prostate-specific antigen level, 8.4 ng/mL, Gleason sum score, 6 and normal digital rectal examination). (a) Axial T2-weighted MRI image through the prostate shows a low signal intensity lesion in the left peripheral zone (arrows). (b–d) Pharmacokinetic maps of calculated K^{trans} (b) and k_{ep} (c) showing increased levels of K^{trans} and k_{ep} in the left peripheral zone. (d) Pharmacokinetic map shows a negative wash-out area (red) in the left peripheral zone. Histopathology after radical prostatectomy revealed a T2a tumor in the left peripheral zone

2.6 Positron Emission Tomography (PET)

Positron emission tomography – the utility of PET scanning with 18-fluorine-labelled deoxyglucose (^{18}F FDG) in detecting prostate cancer is compromised by the relatively low uptake of ^{18}F FDG by prostate cancer cells [42], and significant overlap with marker uptake by benign prostatic hyperplasia, fibrosis and inflammation. Generally, ^{18}F FDG-PET is not recommended for evaluation of the prostate due to sensitivities as low as 4 percent to 64 percent, with a specificity of 50 percent [43-45].

Another tracer – carbon-11 labelled choline (^{11}C -choline) – accumulates in prostatic cells and has the advantage that, unlike ^{18}F FDG, it is not excreted via the urinary tract, and thereby does not interfere with the visualization of the prostate (Fig. 14.7). Furthermore, the prostate is the only organ in the pelvis to accumulate ^{11}C -choline. The ^{11}C -choline uptake was higher in prostate cancer, compared with benign prostatic hyperplasia, but the difference was not statistically significant [46]. Drawbacks are the high costs of ^{11}C -choline and its short, 20-minute half-life.

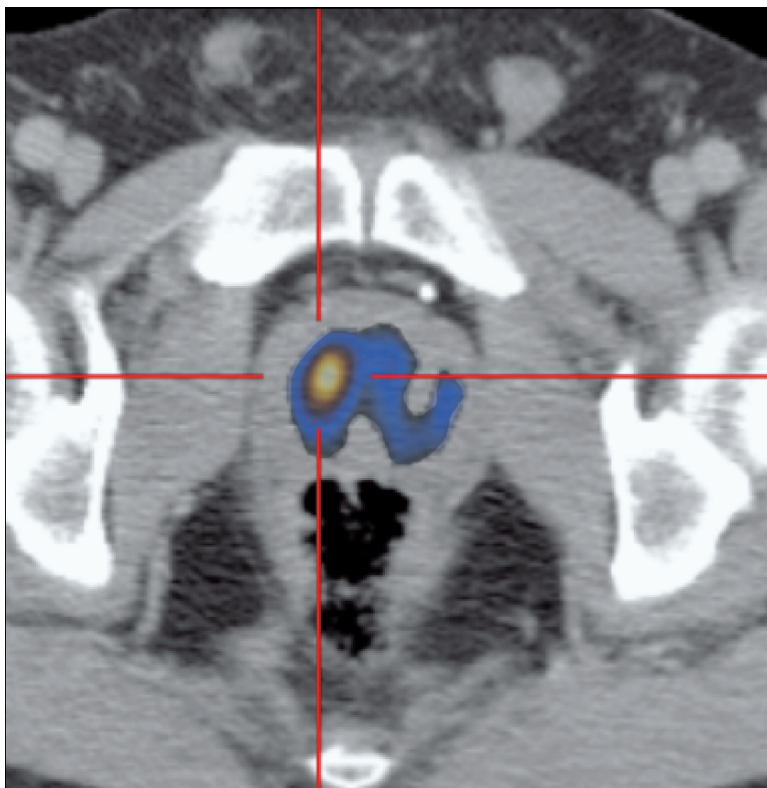


Fig. 14.7 ^{11}C -choline PET-CT image in a 58-year-old patient. ^{11}C -choline uptake is visible in the right central gland which corresponded with a local prostate cancer

2.7 Staging of Prostate Cancer

Clinical staging of prostate cancer currently entails the use of digital rectal examination, PSA as well TRUS. It is now common practice for clinicians treating prostate cancer patients to employ nomograms to determine therapeutic options [47-49]. The most frequently used nomogram, the Partin tables, estimates the chance of organ-confined disease, capsular penetration, seminal vesicle invasion and lymph node metastasis, based on the results of the traditional triad of digital rectal examination, biopsy Gleason score and PSA value [50]. The clinical stage is identified using these variables and is expressed in the TNM staging classification (Table 14.1) [51]. The current general opinion is that localized prostate cancer can be treated successfully by radical prostatectomy or radiation therapy. Nevertheless, advantages of aggressive treatment over watchful waiting in terms of quality-adjusted life expectancy are often small, leading to controversies about the adequate treatment.

Table 14.1 TNM Staging Classification of Prostate Cancer [51]

Stage	
Primary Tumor	
TX	Primary tumor cannot be assessed
T0	No evidence of primary tumor
T1	Clinically the tumor is neither palpable or visible with imaging
T1a	Tumor is an incidental histologic finding in 5 percent or less of tissue resected
T1b	Tumor is an incidental histologic finding in > 5 percent of tissue resected
T1c	Tumor identified with needle biopsy (e.g., because of an elevated PSA)
T2	Tumor confined within the prostate
T2a	Tumor involves one-half of one lobe or less
T2b	Tumor involves more than one-half of one lobe, but not both lobes
T2c	Tumor involves both lobes
T3	Tumor extends through the prostate capsule
T3a	Extra-capsular extension (unilateral or bilateral)
T3b	Tumor invades seminal vesicle(s)
T4	Tumor is fixed or invades adjacent structures other than seminal vesicles: bladder neck, external sphincter, rectum, levator muscles and/or pelvic wall
Regional Lymph Nodes	
NX	Regional lymph nodes were not assessed
N0	No regional lymph node metastasis
N1	Metastasis in regional lymph node(s)
Distant Metastasis	
MX	Distant metastasis cannot be assessed (not evaluated with any modality)
M0	No distant metastasis
M1	Distant metastasis
M1a	Non-regional lymph node(s)
M1b	Bone(s)
M1c	Other site(s) with or without bone disease

Clinical assessment by digital rectal examination and PSA level are not accurate in determining local stage, with underestimations in as many as 40 percent to 60 percent of cases [52, 53]. Accurate staging with additional imaging techniques is, therefore, an important issue for correct management of prostate cancer patients.

TRUS – TRUS may enable correct assessment of locally advanced tumors, but it is not sensitive enough to detect initial extraprostatic extension across the capsule or into the seminal vesicles in clinically confined lesions [54, 55]. Any change of the prostatic capsule, like bulging or irregularity, adjacent to a hypoechoic lesion is suspicious of extracapsular extension. Accuracies of gray-scale TRUS in determining the local disease stage varied from 58 percent to 83 percent, with sensitivities and specificities ranging from 33 percent to 76 percent and 46 percent to 91 percent, respectively [54, 56-59]. Three-dimensional TRUS aids in assessing local disease extension [58]. Duplex Doppler TRUS and contrast-enhanced TRUS are new methods to study tumor vascularity. These blood flow-enhancing TRUS techniques have the potential to improve the local staging of prostate cancer [26]. Future research will indicate their exact role.

CT – Few recent studies have been published on role of CT for staging prostate cancer [60–63]. A pre-radiation therapy staging study of 85 patients showed that CT staging had only a marginal effect on treatment decisions [60]. CT has no use in assessing clinically confined lesions [61]. Two other studies revealed low sensitivity of 26 percent to 29 percent, and specificity of 80 percent to 89 percent [62, 63].

MRI – A large number of studies have been performed over the last two decades to show the accuracy of MRI in local staging of the prostate. Two meta-analyses on local staging by MRI found combined maximum sensitivities and specificities of 71 percent to 74 percent, while sensitivity was 62 percent to 69 percent at a specificity of 80 percent [64, 65]. T2-weighted MRI in more than one plane, as well as utilizing an endorectal coil, resulted in significantly better staging performance. The use of endorectal-pelvic phased array coils is recommended. Significant improvement of anatomic details, extracapsular extension accuracy and specificity was found when an endorectal-pelvic phased-array coil is used [53]. MRI should be performed at least four weeks after prostatic biopsy. T1-weighted sequence should be acquired for evaluation of post-biopsy hemorrhage.

The most reliable criteria for the detection of extracapsular extension of prostate carcinoma are asymmetry of the neurovascular bundle (Fig. 14.8), obliteration of the rectoprostatic angle and tumor bulge into the periprostatic fat (Fig. 14.9) [66]. Seminal vesicles on T2-weighted images appear as tubular structures with thin hypo-intense walls and filled with hyper-intense fluid. The diagnosis of seminal vesicle invasion is made when focal or diffuse thickening (hypo-intense) of the tubular walls, associated with focal hypo-intense luminal lesions, is present (Fig 14-10).

The most cost-effective patient group to undergo local staging with endorectal MRI are those considered to have an intermediate risk of T3 disease, based on PSA level (between 4 to 20 ng/mL), and a Gleason score of five to seven [67]. Jager, et al. developed a decision analysis model that supported the position that MRI in the pre-operative work-up of prostate cancer is cost-effective in patients with a moderate to high chance of extra-capsular disease, and should be performed with an emphasis on

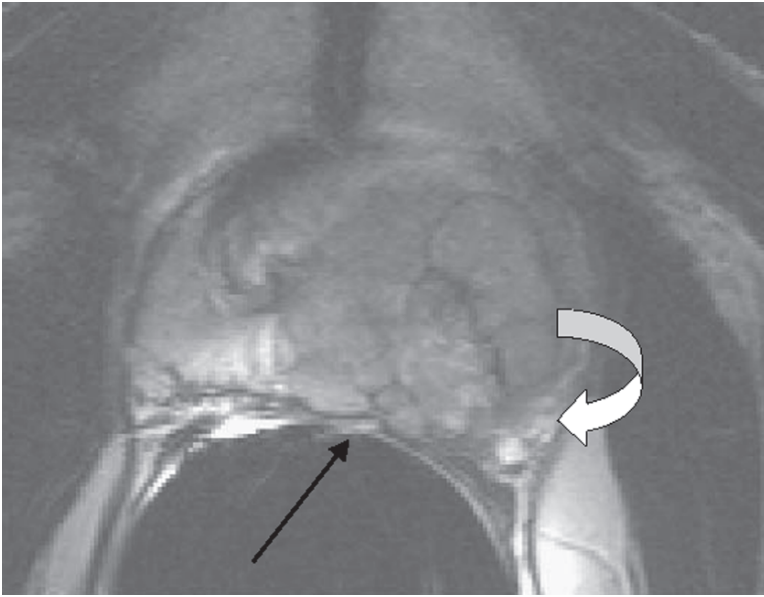


Fig. 14.8 60-year-old man with stage T3a disease (T) in the left peripheral zone and central gland. T2-weighted MRI image shows invasion of the neurovascular bundle (*curved arrow*). Obliteration of the left rectoprostatic angle (*arrow*), but the right neurovascular bundle and rectoprostatic angle are intact

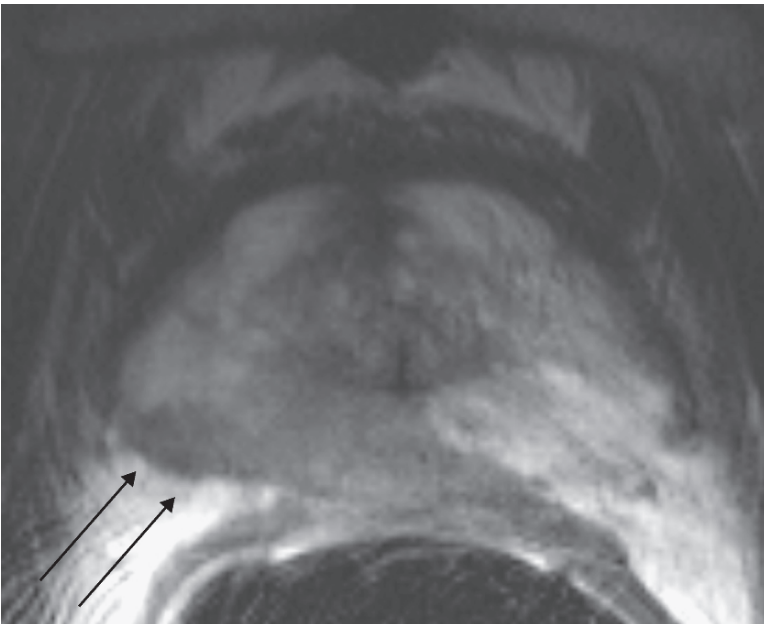


Fig. 14.9 51-year-old man with stage T3a disease in the right peripheral zone. T2-weighted MRI image shows that the tumor (T) has lower signal intensity than the normal peripheral zone and shows bulging (*arrows*) and broad surface contact with capsule



Fig. 14.10 Seminal vesicle invasion in 58-year-old patient. Axial T2-weighted MRI image through seminal vesicles shows a low signal intensity within the lumen of the seminal vesicles and thickening of the tubular walls

achieving high specificity [68]. Langlotz, et al. emphasized the need of high-specificity reading in prostate MRI to ensure that as few patients as possible are unnecessarily denied potential curative therapy because of false positive MRI results [69].

A substantial improvement in overall staging accuracy of endorectal MRI can be achieved by careful pathologic correlation and by considering the anatomic features of prostate cancer. A prospective study of 103 patients revealed a significant improvement in staging performance for the less experienced reader using multislice dynamic contrast-enhanced MRI [70]. Also, the addition of three-dimensional MRSI to MRI improved staging accuracies, particularly for less experienced readers [71]. Imaging at higher magnetic field strengths (e.g., 3 tesla) results in increased anatomical resolution. Two recent studies on local staging with 3T MRI reported a sensitivity and specificity of 80 percent to 88 percent and 94 percent to 100 percent, respectively [72, 73].

Positron emission tomography – The role of ^{18}F FDG-PET in local staging is very limited due to this technique's low spatial resolution and the low uptake within the primary tumor [74].

2.8 *Lymph Node Staging*

Pelvic lymph node metastases have a significant effect on the prognosis of patients with malignancies. One positive lymph node can turn prostate cancer from a local to a systemic disease unsusceptible to curative treatment [75, 76]. Surgical open pelvic lymph node dissection with histopathological examination is currently the most reliable method of assessing lymph node status.

Abdominal ultrasound plays no role in this phase of staging [77]. Routine cross-sectional imaging modalities, such as CT and MRI, have a limited sensitivity in identifying metastases [78-80]. CT and MRI interpretation of lymph nodes is essentially based on size and shape criteria. These techniques only use the size (8 to 10mm) and shape (round – oval) criteria and, therefore, are limited [80]. In a study of 80 patients, Harisinghani, et al. found a 35 percent sensitivity and 90 percent specificity of detection of positive lymph nodes using anatomical MRI node-by-node [81].

MR lymphangiography (MRL) uses intravenously administered lymphotropic ultrasmall superparamagnetic iron-oxide (USPIO) particles (Ferumoxtran-10) with a long plasma circulation time and is a novel, non-invasive cellular imaging tool for the evaluation of nodal involvement. MRL is an accurate tool to differentiate benign from malignant lymph nodes [82, 83]. Post-ferumoxtran-10 MRI exam includes both a sequence which is insensitive for iron using T1- or proton-weighted turbo spin echo sequences, and a sequence which is sensitive for iron (Fig. 14.11). For the latter purpose, a good sequence is a high resolution T2-weighted gradient echo sequence. Ferumoxtran-10-enhanced MRI achieved a 97.3 percent accuracy with high sensitivity (90.5 percent) and specificity (97.8 percent) on a node-by-node basis [81]. Harisinghani, et al. achieved a sensitivity of 100 percent and a specificity of 96 percent for detection of 5 to 10mm nodes with 1.5T MRI. However, when the metastatic lymph node was smaller than 5mm, this sensitivity dropped to 41 percent. Ferumoxtran-10-enhanced MRI at a 3T field strength using a higher spatial resolution with improvement of image quality may allow detection of small metastatic nodes (<5mm) in the future [84].

Although very promising in metastatic lung cancer, the role of ^{18}F FDG-PET scanning is limited in the urinary tract region, as ^{18}F -fluorodeoxyglucose accumulates in the urinary bladder and kidneys. This makes an evaluation of metastases at these sites difficult. In prostate cancer this method is further limited by its low uptake in metastatic nodes. Although the sensitivity of ^{18}F FDG-PET is slightly better (67 percent), compared to those of CT and unenhanced MRI, this value is, however, not high enough to replace pelvic lymph node dissection (Fig. 14.12) [85].

2.9 *Metastatic Bone Disease*

The first diagnostic test to detect or exclude bone metastases is the technetium-99m-diphosphonate bone scintigraphy (Fig 14.13). A meta-analysis of 23 prostate cancer studies deduced detection rates of 2.3 percent, 5.3 percent and 16.2 percent for patients with PSA levels below 10 ng/mL, between 10 and 19.9 ng/mL

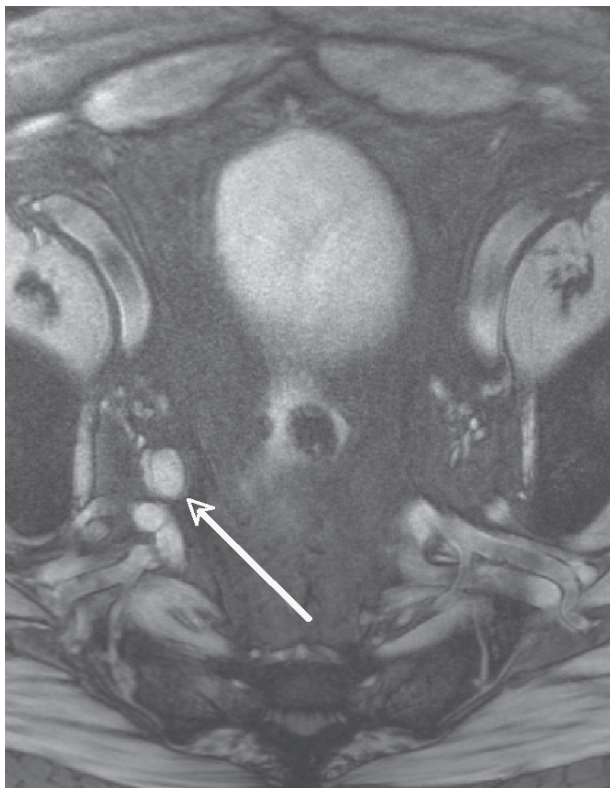


Fig. 14.11 Normal size lymph node (8 mm) in the right obturator fossa in a 60-year-old male with biopsy proven prostate cancer (PSA 15.3 ng/mL; Gleason score 7). On post ferumoxtran-10 T2-weighted gradient echo MRI image (which is iron sensitive) this normal sized node remains white (circle). On histopathology this node was completely metastatic

and between 20 to 49.9 ng/mL, respectively [86]. In a large study it was found that, in patients with levels below 20 ng/mL, the false negative rate was less than 2 percent [87]. Bone scintigraphy lacks specificity and, thus, primary skeletal diseases may cause false positive findings. X-ray can be used to exclude false positive findings on bone scintigraphy due to conditions such as trauma, degenerative joint disease or other chronic diseases. Conventional X-rays are too insensitive for the detection of metastatic bone lesions. Most metastatic bone lesions are sclerotic [88]. A 50 percent change in bone mineral density is needed for metastatic bone lesions to be visible on X-ray images [89]. CT has no place in determining metastatic bone disease.

The high spatial resolution and excellent soft tissue contrast make MRI an ideal tool for the detection of osseous lesions. Whole-body MRI appears to be a very sensitive tool to determine bone marrow metastases and, in less than 15 minutes, is feasible for tumor staging [90]. Advantages of MRI are the absence of radiation exposure, as well as the ability to also detect non-skeletal metastases.

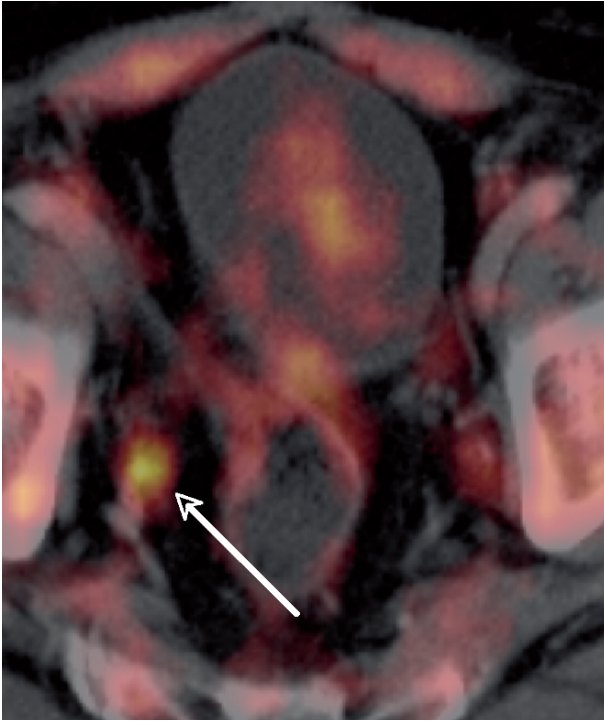


Fig. 14.12 ¹¹C-choline PET-CT image of the same patient as in Fig. 14.11. The metastatic node in right obturator fossa demonstrated uptake of ¹¹C-choline. This is indicative of lymph node metastasis

Purely sclerotic lesions take up ¹⁸F-FDG less avidly, compared to purely lytic or mixed metastases. Bone metastases in prostate cancer are commonly sclerotic lesions. ¹⁸F-FDG-PET is considered to be inferior to bone scintigraphy [91]. An important role of PET imaging may lie in its early ability to detect treatment response in patients with metastatic disease who are receiving chemotherapy.

2.10 Conclusions

TRUS remains the primary imaging tool for the detection of prostate cancer and for guiding prostate biopsy. Functional MRI achieves high localization rates. MRI of the prostate can be used as a problem-solving tool in patients with rising PSA and repetitive negative biopsies. MRI at 1.5T, using an endorectal coil combined with a pelvic phased-array coil, is currently the optimal choice for determining the local disease stage in prostate cancer patients. Dynamic contrast-enhanced MRI and MR spectroscopic imaging may be used to increase the staging accuracy for less experienced readers. The



Fig. 14.13 Technetium-99m-diphosphonate bone scintigraphy in a patient with bone metastases (PSA 82ng/mL). Anterior and posterior whole body delayed planar imaging was performed. Planar bone scan imaging demonstrates a substantial focus of increased uptake at the level of thoracic spine level 2/3/4, as well as at the left aspect of the approximate T7 and T12. There is also moderate increased focal uptake at L3, the right sacroiliac joint, sacrum, as well as the level of the fifth (left) and seventh (right) rib

role of PET in local staging is limited. MR lymphangiography using ultrasmall superparamagnetic iron-oxide particles is the most sensitive and specific method for detecting lymph node metastases. Bone scintigraphy is the most sensitive method for detection of bone metastases. However, FDG-PET and whole body MRI are promising modalities for detection and assessment of response to therapy.

Key Points

- The urologic work-up in patients with elevated PSA consists of a digital rectal examination and transrectal ultrasound.
- Transrectal ultrasound is the primary imaging tool for the detection of prostate cancer.

- More than 70 percent of adenocarcinoma of the prostate arises in the peripheral zone, whereas about 20 percent emerge in the transitional zone and 10 percent in the central zone.
- Computed tomography should not be used for prostate cancer detection, localization and staging.
- Dynamic contrast-enhanced MRI and MR spectroscopic imaging can be used for localization of prostate cancer, and to increase the staging accuracy for less experienced readers.
- The optimal sensitivity and specificity for the detection of lymph node metastases is achieved by using MRI using ultra-small superparamagnetic iron-oxide particles.
- Bone scintigraphy remains the single most sensitive method of detecting bone metastases.

2.11 Testicular Cancer

Testicular germ cell cancer accounts for only 1 percent of all cancer in males [92]. The peak prevalence occurs between 25 and 35 years of age. The incidence of testicular cancer has doubled in the last 40 years. Bilateral tumors are found in 0.7 percent of men with germ cell tumors at diagnosis, and 1.5 percent of patients develop metachronous lesions within five years [93].

Once the leading cause of cancer death in men between 15 and 35 years of age, it has now proved to be a model of success with a five-year survival rate exceeding 95 percent [94]. This success in treatment is related to improved staging and treatment methods. Imaging plays a central role in assessment of tumor bulk, sites of metastases, monitoring response to therapy, surgical planning and accurate assessment of disease at relapse [95].

2.12 Clinical Symptoms of Testicular Cancer

The most common sign of testicular germ cell cancer is a painless unilateral mass in the scrotum, which is inseparable from the testis (up to 95 percent of cases)[96]. In 20 percent of the cases, the first symptom is scrotal pain, followed by back and flank pain in 11 percent. Gynecomastia appears in 7 percent of the cases [97]. Although differential diagnosis must be established with any other intrascrotal mass or disease, any scrotal complaint at a young age needs to be thoroughly investigated to rule out testicular germ cell cancer.

2.13 Pathology of Testicular Germ Cell Cancer

Ninety-five percent of all testicular tumors are germ cell tumors (Fig. 14.14). The remaining are lymphomas (4 percent) and Leydig or Sertoli cell tumors. Testicular

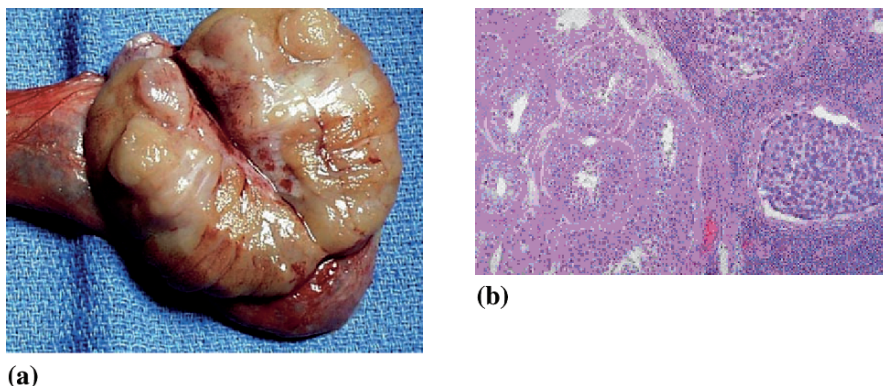


Fig. 14.14 (a) Seminomatous germ cell cancer. (b) Histopathology of normal testis (left) with adjacent seminomatous germ cell cancer (right)

germ cell tumors are derived from spermatogenic cells and may be classified as unipotential or totipotential. Unipotential tumors are seminomas, which comprise 35 percent to 50 percent of all germ cell tumors. Nonseminomatous germ cell tumors are considered to be totipotential.

Serum tumor markers are especially helpful to differentiate germ cell tumors from each other and from other malignancies. Serum concentrations of alpha-feto-protein (AFP) and/or beta-human chorionic gonadotropin (beta-hCG) are elevated in 80 percent to 85 percent of non-seminomas. In contrast, serum beta-hCG is elevated in fewer than 25 percent of testicular seminomas, and AFP is not elevated in pure seminomas. However, these tumor markers cannot accurately assess disease bulk or locate sites of tumor spread [95].

2.14 Diagnosis of Testicular Cancer

The first step in diagnosing testicular cancer is usually through self-examination. Testicular ultrasound is used to confirm the presence of a testicular mass (Fig. 14.15), to distinguish from other scrotal abnormalities and to explore the contralateral testis [98-102]. The sensitivity of testicular ultrasound in detecting testicular tumors is almost 100 percent [103]. Furthermore, ultrasound is almost 100 percent sensitive in differentiating intratesticular from extratesticular lesions [102, 104, 105] and is able to detect microlithiasis (Fig. 14.16). Extratesticular lesions are commonly benign in adults, whereas in children these lesions are often malignant [106]. Microlithiasis should be cautiously followed up, since it can be associated with testicular germ cell cancer [107]. Serum tumor markers contribute to the diagnosis. At the time of the diagnosis a chest radiography is used to evaluate the mediastinum for lymphadenopathy, and the lungs for haematogenous metastases. After a testicular tumor has been clinically diagnosed, the inguinal ablation of the testis is indicated (Fig. 14.17).

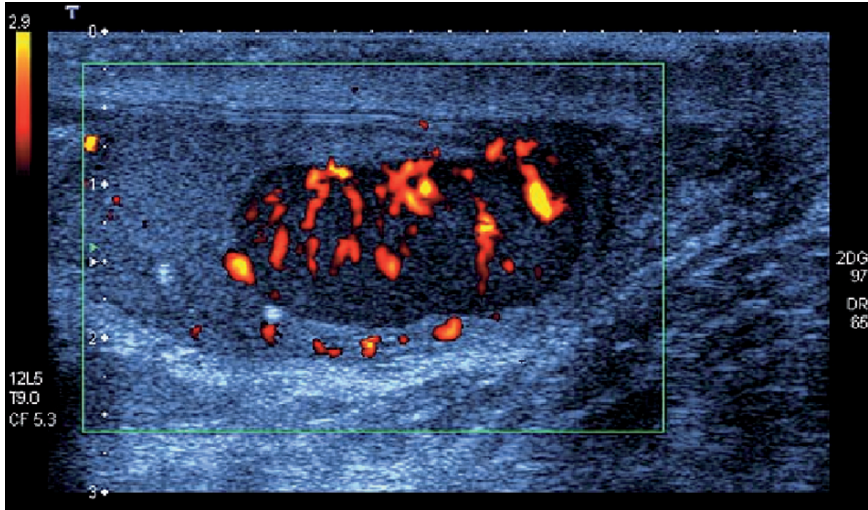


Fig. 14.15 Testicular ultrasound of a testis with increased vascular flow at the cancerous part

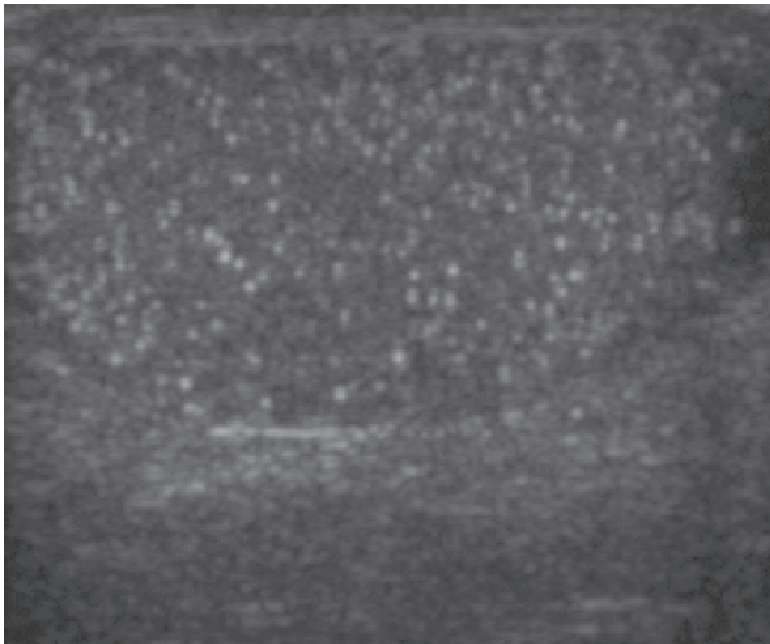


Fig. 14.16 The appearances of testicular microlithiasis ('snow storm' appearance on ultrasound)



Fig. 14.17 Right-sided inguinal orchiectomy. The incision is high inguinal and the whole spermatic cord should be removed up to the internal ring with separation of ductus deferens and gonadal vessels

2.15 Staging of Testicular Cancer

As soon as the diagnosis of germ cell cancer has been pathologically confirmed, further staging examinations are warranted to examine the extent of disease. Staging is of utmost importance as it is the cornerstone for further treatment after orchiectomy. The European Germ Cell Cancer Consensus Group (EGCCCG) recommends that TNM staging be used [51] (Table 14.2). The most commonly used staging system in Europe for dissemination is the Royal Marsden Hospital Classification system (Table 14.3) [108]. Today, computerized tomography (CT) of the abdomen and chest is the standard technique in initial staging.

The most common sites for metastases are via the lymphatic system to the retroperitoneal nodes, and via the hematogenous route to the lungs and, less commonly, to the liver, brain and bone. In general, advanced stage disease will be treated primarily with chemotherapy. Nonseminoma germ cell tumors appear as multiple small peripheral nodules, whereas seminoma metastases tend to be larger masses [95]. Other sites of hematogenous metastases, though rarely seen and usually only in the setting of advanced disease, include the adrenals, kidneys, spleen, pleura, pericardium and peritoneum [95].

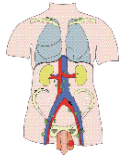
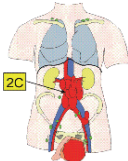
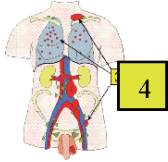
Lymphatic spread occurs via lymphatic channels (from spermatic cord and testicular vessels to retroperitoneal lymph nodes). Usually, right-sided testicular neoplasms spread to the right side of the retroperitoneum. Lymph node metastases can be

Table 14.2 TNM Staging Classification of Testicular Tumors [51]

Stage	
Primary Tumor	
<i>The extent of the primary tumor is classified after radical orchidectomy (pT)</i>	
pTX	Primary tumor cannot be assessed (if no radical orchidectomy has been performed, TX is used)
pT0	No evidence of primary tumor (e.g., histological scar in testis)
pTis	Intratubular germ cell neoplasia
pT1	Tumor limited to testis and epididymis without vascular/lymphatic invasion; tumor may invade into the tunica albuginea, but not the tunica vaginalis
pT2	Tumor limited to testis and epididymis with vascular/lymphatic invasion, or tumor extending through tunica albuginea with involvement of tunica vaginalis
pT3	Tumor invades spermatic cord with or without vascular/lymphatic invasion
pT4	Tumor invades scrotum with or without vascular/lymphatic invasion
Regional Lymph Nodes	
<i>Clinical Involvement</i>	
NX	Regional nodes cannot be assessed
N0	No regional lymph node metastasis
N1	Metastasis with a lymph node mass ≤ 2 cm in greatest dimension or multiple lymph nodes none > 2 cm in greatest dimension
N2	Metastasis with a lymph node mass > 2 cm, but < 5 cm in greatest dimension, or multiple lymph nodes, any one mass > 2 cm, but ≤ 5 cm in greatest dimension
N3	Metastasis with a lymph node mass > 5 cm in greatest dimension
<i>Pathological Involvement</i>	
pN0	No regional lymph node metastases
pN1	Metastasis with a lymph node mass ≤ 2 cm in greatest dimension and five or fewer positive nodes, none > 2 cm in greatest dimension
pN2	Metastasis with a lymph node mass > 2 cm, but ≤ 5 cm in greatest dimensions; or more than five nodes positive, none > 5 cm; or evidence of extranodal extension of tumor
pN3	Metastasis with a lymph node mass > 5 cm in greatest dimension
<i>Distant Metastases</i>	
MX	Distant metastasis cannot be assessed
M0	No distant metastasis
M1	Distant metastasis
M1a	Non-regional lymph node or pulmonary metastasis
M1b	Distant metastasis other than to non-regional lymph nodes and lungs

identified around the inferior vena cava, and between the level of right renal hilum and the aortic bifurcation. Lymph node metastases of left-sided testicular cancer may be found adjacent to the abdominal aorta and just below the left renal vein. Contralateral involvement is uncommon, but may occur with a larger disease burden [109]. Pelvic lymphadenopathy is uncommon in the absence of bulky disease [110].

Table 14.3 The Royal Marsden Hospital Classification System for Germ Cell Tumors

Stage I	Tumor limited to testis	
Stage II	Infradiaphragmatic lymph node involvement	
IIA	Metastases <2 cm in diameter	
IIB	Metastases 2 to 5 cm in diameter	
IIC	Metastases 5 to 10 cm in diameter	
IID	Metastases >10 cm in diameter	
Stage III	Supradiaphragmatic lymph node involvement	
A-D	See stage II	
Stage IV	Extralymphatic involvement of lung (L), liver (H), brain and bone	

2.16 Ultrasound

Testicular ultrasound (linear 6 to 12 MHz probe) is performed in at least two planes. The homogenous, low-to-medium echogenicity of the testicle noted in boys increases after puberty [111]. Testicular tumors are usually well defined and hypoechoic relative to the normal testicle. Some testicular tumors may show a heterogeneous echotexture, calcification or cystic change. Color and power Doppler ultrasound may be helpful in delineating areas of malignant involvement, but this is not specific and may not be demonstrated in small tumors [112]. If a malignant-appearing mass is encountered, sonography of the retroperitoneum may identify associated lymphadenopathy [113].

2.17 Computed Tomography

Computed tomography (CT) is used for staging metastatic disease and for follow-up after therapy in patients with disseminated disease. The abdominal CT examination offers a sensitivity of 30 percent to 35 percent in the evaluation of retroperitoneal lymph nodes in the landing zone by using a threshold of 1 cm. Contrast-enhanced

CT of the thorax, abdomen and pelvis is recommended according to the guidelines of the EGCCCG. CT of the brain is only performed in patients with suspected disease and patients with high risk factors for metastases. CT is limited in distinguishing residual tumors from hematoma, fibrosis and/or necrosis [113].

2.18 Magnetic Resonance Imaging

Magnetic resonance imaging (MRI) can be used as a problem-solving tool in inconclusive ultrasound cases. MRI is performed in supine positioning and surface coils (phased-array) are positioned above the testicles. T1- and T2-weighted sequences in at least two planes are acquired. Dynamic contrast-enhanced subtraction MRI can be used to differentiate testicular diseases from scrotal disorders [114].

The normal testicle has an intermediate homogenous signal intensity on T1-weighted images, and homogeneous high signal intensity (less than fluid signal intensity) on T2-weighted images. Signal intensity of the epididymis is low signal intensity on both T1- and T2-weighted images. The tunica albuginea and testicular septa appear as low signal intensity structures [115].

Testicular neoplasms present with low signal intensity on T2-weighted images and intermediate to low signal intensity on T1-weighted images. MRI cannot predict the histological type [116].

2.19 Positron Emission Tomography (PET)

Examining the role of 18-fluorine-labelled deoxyglucose ^{18}F -FDG-PET in testicular germ cell cancer (Fig. 14.18) shows a sensitivity of 82 percent, a specificity of 94 percent, and a negative predictive value of 94 percent [117-120]. However, lymph node metastases smaller than 1 cm can be missed with ^{18}F -FDG-PET. Seminomatous germ cell tumors have a significantly higher uptake of FDG, compared to nonseminomatous lesions. The role of ^{18}F -FDG-PET in primary staging is minimal if metastatic disease has already been diagnosed [95]. ^{18}F -FDG-PET is of incremental value in assessing residual disease or recurrence [121].

2.20 Imaging in Clinical Stage I Testicular Cancer

Patients with clinical stage I tumors have disease that is confined to the testis. However, approximately 30 percent of the clinical stage I non-seminomas are understaged by radiological imaging, and are found to have metastatic disease at retroperitoneal surgery [122].

The abdominal CT scan offers a sensitivity of 30 percent to 35 percent in the evaluation of retroperitoneal lymph nodes in the landing zone by using a threshold

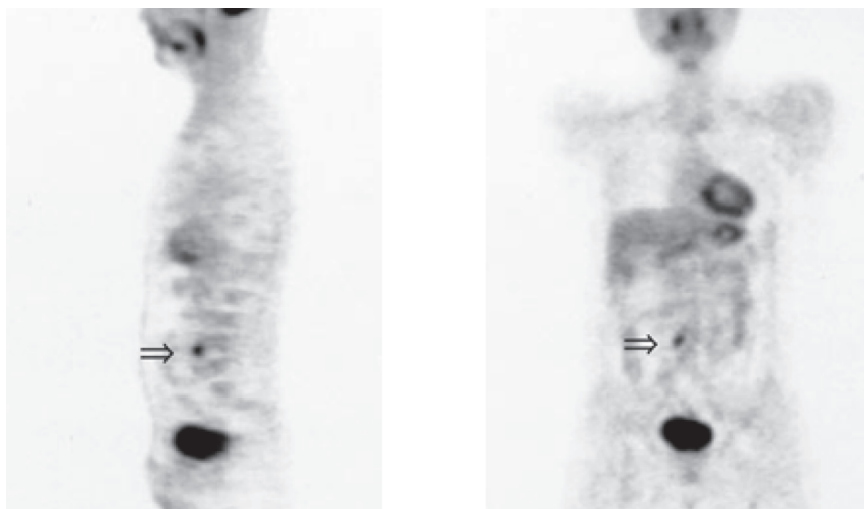


Fig. 14.18 Patient with a nonseminomatous testicular cancer. Through clinical imaging a lesion of 9mm was found on CT. Increased uptake of ^{18}F FDG suggests the presence of a retroperitoneal metastasis

of 1 cm. Lowering this threshold results in an increased sensitivity, but a decreased specificity (with a criterion of 4 mm, the sensitivity increases to 93 percent, but the specificity decreases to 58 percent) [123]. New generation CT scans do not seem to improve the sensitivity [124]. Although pulmonary involvement rarely occurs in the absence of retroperitoneal disease, a chest X-ray is mandatory and the preferred imaging modality. Routine CT of the chest, although highly sensitive, produces a significant number of false positive scans (detecting 2 mm sized lesions, but 70 percent of those are benign) [125].

Alternative imaging methods like PET and MRI add little to the management of clinical stage I non-seminoma germ cell cancer. The accuracy of MRI is in line with CT examination [126-127]. Currently, the additional value of intravenous ferumoxtran-10 administration before MRI has been evaluated. Ferumoxtran-10 is an ultrasmall nanoparticle given intravenously, which moves into the reticulo-endothelial system. Benign nodes only take up ferumoxtran-10, leaving the cancerous lymph nodes without enhancement. Ferumoxtran-10-enhanced MRI yields a higher sensitivity and specificity when compared with unenhanced MRI (sensitivity: 88.2 percent vs 70.5 percent, specificity: 92 percent vs 68 percent). Although the results are encouraging, the precise role of this tool in clinical stage I testicular germ cell cancer remains to be determined [128].

The old-fashioned method of imaging lymph nodes through lymphangiography has gained new interest via new contrast agents. Lymphangiography allows visualization of the three main lymphatic channels (paracaval, interaortacaval and paraaortal, Fig. 14.19). The major goal of the new contrast agents is to investigate the feasibility and accuracy of radio-guided mapping of sentinel lymph nodes (SLNs) in clinical

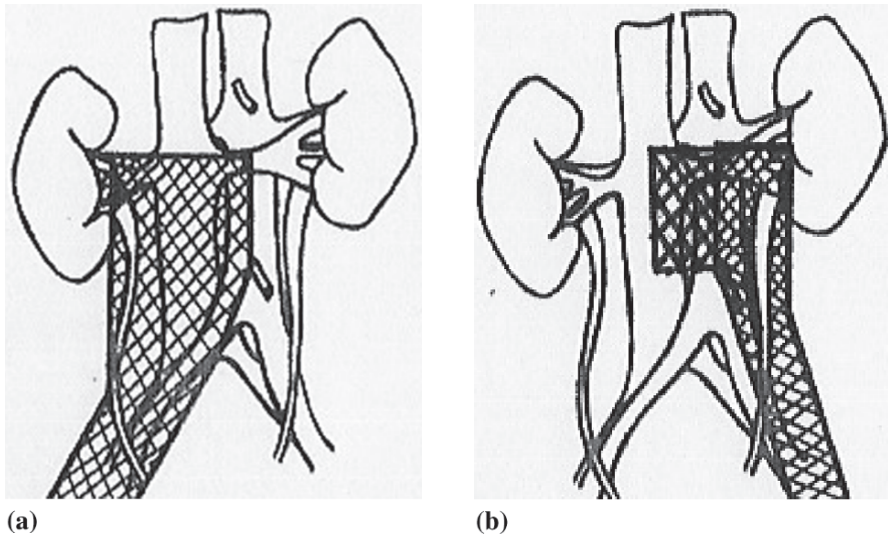


Fig. 14.19 Landing zone for retroperitoneal metastases of testicular germ cell cancer. In patients with right-sided tumors **(a)**, the limits of dissection for the modified nerve-sparing template include the right ureter, the renal veins, the right lateral wall of the aorta, the inferior mesenteric artery and the iliac bifurcation. For left-sided tumors **(b)**, the limits of dissection are the left ureter, left renal vein, left mid-wall of vena cava, the inferior mesenteric artery and iliac bifurcation

Stage I testicular tumors. For a left-sided testicular tumor the primary landing zone (e.g., SLN) includes the nodes in the para-aortic region below the renal vessels and the ipsilateral lateral distribution of the para-aortic, pre-aortic and left common iliac nodes. For right-sided tumors the primary landing zone is in the interaortacaval region below the renal vessels and the ipsilateral lymph nodes in the paracaval, preaortic and right common iliac region. Satoh, et al. injected (99m) Technetium-labeled phytate around the testicular tumor in 22 patients. In 21 of them the SLN was detected by laparoscopic retroperitoneal lymph node dissection. Only in two patients were micrometastases found in the SLN. Both patients were free of disease after adjuvant chemotherapy [129]. As in two other patients lymph node relapses were detected, the real value of radio-guided mapping of SLNs with laparoscopy can be questioned.

In clinical stage I seminomas approximately 15 percent of patients have sub-clinical metastatic disease [130]. In accordance with nonseminomas, FDG-PET and MRI provide no additional value above CT scan. [118, 128, 131]

2.21 Imaging in Advanced Stage Testicular Germ Cell Cancer

The most common sites for metastases are via the lymphatic system to the retroperitoneal nodes, and via the hematogenous route to the lungs and, less commonly,

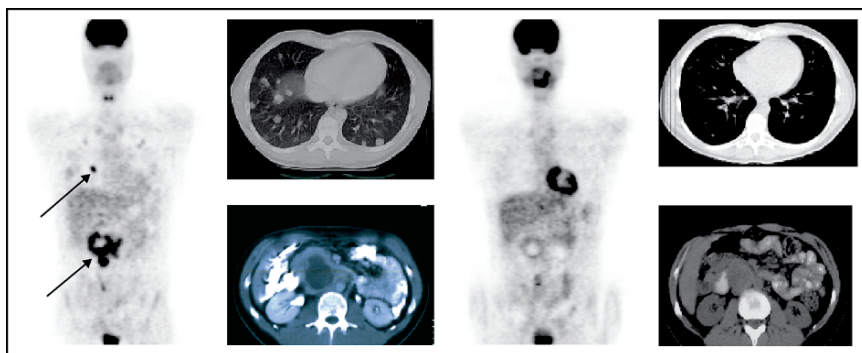


Fig. 14.20 Coronal ^{18}F FDG-PET scan shows metastases of nonseminomatous testicular germ cell tumor in the retroperitoneum, and in lungs with increased uptake of ^{18}F FDG (arrow). The lesion in the retroperitoneum shows no uptake in the center. The patient showed partial radiological response during treatment: both decrease in ^{18}F FDG uptake and volume reduction on CT scan retroperitoneally, and disappearance of lung metastases. Surgery of residual retroperitoneal mass showed necrotic and teratomatous tissue in the center, and inflammatory tissue at the rim of the retroperitoneal mass

to the liver, brain and bone. In general, advanced stage disease will be treated primarily with chemotherapy. Today, CT is the standard in initial staging. Though FDG-PET has the potential to improve clinical staging, more studies are warranted to establish its definitive value [131, 132].

Following completion of chemotherapy, residual tumorous lesions are found in up to 15 percent of patients with seminomas [133], compared to 20 percent of patients with non-seminomas [134]. Furthermore, 40 percent of the nonseminomatous residual masses contain mature teratoma (pre-malignant disease). The key to success is complete surgical removal of these masses. A major challenge is finding the optimal method for differentiating patients with post-chemotherapy (pre-) malignant residual masses from those with fibrotic lesions. Again, CT and the change in size of the mass has been the standard for assessing residual masses. PET is of incremental value in assessing residual seminomatous disease. A study of 56 scans by De Santis, et al. reveals that PET had a sensitivity, specificity, positive predictive value and negative predictive value of 100 percent, 80 percent, 100 percent and 96 percent, respectively, versus 74 percent, 70 percent, 37 percent and 90 percent for CT [121]. In contrast, in nonseminomas there is no real additional value as PET cannot differentiate between fibrosis and mature teratoma (Fig. 14.20) [119].

2.22 *Follow-up of Testicular Germ Cell Cancer*

Because most recurrences after curative therapy will occur in the first two years, follow-up should be most frequent and intensive during this time. Follow-up protocols

vary by institution and by type, stage and treatment of the primary disease. After treatment all patients receive follow-up care through regular outpatient visits, during which physical examination, serum tumor markers, chest X-ray and CT scans are performed. Currently, efforts are made to optimize the follow-up schedule. [135,136]

2.23 Conclusions

Ultrasound is the initial investigative tool with regard to scrotal masses. Patients should undergo a CT examination of the chest, abdomen and pelvis when the histological diagnosis of testicular germ cell cancer has been confirmed.

Clinical staging is hampered by the inability to detect micrometastatic disease because the sensitivity of conventional imaging studies is inversely proportional to tumor volume. To date, the metabolic tracer imaging studies have no additional value because the micrometastases do not show enough metabolic activity for detection. In re-assessing the extent of metastatic disease after chemotherapy, CT scan remains the first choice of imaging. PET can contribute to the management of residual seminoma lesions.

References

1. Jemal A, Siegel R, Ward E, Murray T, Xu J, Thun MJ. Cancer statistics, 2007. *CA Cancer J Clin* 2007; 57(1); 43-66.
2. Carter HB, Piantadosi S, Isaacs JT. Clinical evidence for and implications of the multi-step development of prostate cancer. *J Urol* 1990; 143:742-746.
3. Parkin DM, Bray FI, Devesa SS. Cancer burden in the year 2000. The global picture. *Eur J Cancer* 2001; 37 Suppl 8:S4-66.
4. Konety BR, Bird VY, Deorah S, Dahmouh L. Comparison of the incidence of latent prostate cancer detected at autopsy before and after the prostate specific antigen era. *J Urol* 2005; 174:1785-1788.
5. McNeal JE. Normal anatomy of the prostate and changes in benign prostatic hypertrophy and carcinoma. *Semin Ultrasound CT MR* 1988; 9:329-334.
6. Coakley FV, Hricak H. Radiologic anatomy of the prostate gland: a clinical approach. *Radiol Clin North Am* 2000; 38:15-30.
7. Sattar AA, Noël J-C, Vanderhaeghen J-J, Schulman CC, Wespes E. Prostate capsule: computerized morphometric analysis of its components. *Urology* 1995; 46:178-181
8. Greenhalgh R, Kirby RS. Anatomy and physiology of the prostate and benign prostatic hyperplasia. *Atlas Urol Clin* 2002; 10:1-9
9. Richie JP, Catalona WJ, Ahmann FR, et al. Effect of patient age on early detection of prostate cancer with serum prostate-specific antigen and digital rectal examination. *Urology* 1993; 42:365-374.
10. Schröder FH, van der Maas P, Beemsterboer P, et al. Evaluation of the digital rectal examination as a screening test for prostate cancer. Rotterdam section of the European Randomized Study of Screening for Prostate Cancer. *J Natl Cancer Inst.* 1998; 90:1817-1823.

11. Philips TH, Thompson IM. Digital rectal examination and carcinoma of the prostate. *Urol Clin North Am.* 1991; 18:459-465.
12. Freedland SJ, Mangold LA, Epstein JI, Partin AW. Biopsy indicator –a predictor of pathologic stage among men with preoperative serum PSA levels of 4.0ng/mL or less and T1c disease. 2004; 63(5):887-891.
13. Lee F, Gray JM, McLeary RD, et al. Prostatic evaluation by transrectal sonography: criteria for diagnosis of early carcinoma. *Radiology* 1986; 158:91-95.
14. Meirelles LR, Billis A, Cotta AC, Nakamura RT, Caserta NM, Prando A. Prostatic atrophy: evidence for a possible role of local ischemia in its pathogenesis. *Int Urol Nephrol* 2002; 34:345-350.
15. Ellis WJ, Brawer MK. The significance of isoechoic prostatic carcinoma. *J Urol* 1994; 152:2304-2307.
16. Heijmink SW, van Moerkerk H, Kiemeny LA, Witjes JA, Frauscher F, Barentsz JO. A comparison of the diagnostic performance of systematic versus ultrasound-guided biopsies of prostate cancer. *Eur Radiol* 2006; 16:927-938.
17. Hodge KK, McNeal JE, Terris MK, Stamey TA. Random systematic versus directed ultrasound guided transrectal core biopsies of the prostate. *J Urol* 1989; 142:71-74.
18. Gore JL, Shariat SF, Miles BJ, et al. Optimal combinations of systematic sextant and laterally directed biopsies for the detection of prostate cancer. *J Urol* 2001; 165:1554-1559.
19. Scherr DS, Eastham J, Ohori M, Scardino PT. Prostate biopsy techniques and indications: when, where, and how? *Semin Urol Oncol* 2002; 20:18-31.
20. Djavan B, Remzi M, Schulman CC, Marberger M, Zlotta AR. Repeat prostate biopsy: who, how and when?. a review. *Eur Urol* 2002; 42:93-103.
21. Wilson NM, Masoud AM, Barsoum HB, Refaat MM, Moustafa MI, Kamal TA. Correlation of power Doppler with microvessel density in assessing prostate needle biopsy. *Clin Radiol* 2004; 59:946-950.
22. Okihara K, Kojima M, Nakanouchi T, Okada K, Miki T. Transrectal power Doppler imaging in the detection of prostate cancer. *BJU Int* 2000; 85:1053-1057.
23. Rifkin MD, Sudakoff GS, Alexander AA. Prostate: techniques, results, and potential applications of color Doppler US scanning. *Radiology* 1993; 186:509-513.
24. Lavoipierre AM, Snow RM, Frydenberg M, et al. Prostatic cancer: role of color Doppler imaging in transrectal sonography. *AJR Am J Roentgenol* 1998; 171:205-210.
25. Frauscher F, Klauser A, Volgger H, et al. Comparison of contrast enhanced color Doppler targeted biopsy with conventional systematic biopsy: impact on prostate cancer detection. *J Urol* 2002; 167:1648-1652.
26. Pelzer A, Bektic J, Berger AP, et al. Prostate cancer detection in men with prostate specific antigen 4 to 10ng/ml using a combined approach of contrast enhanced color Doppler targeted and systematic biopsy. *J Urol* 2005; 173:1926-1929.
27. Halpern EJ, Ramey JR, Strup SE, Frauscher F, McCue P, Gomella LG. Detection of prostate carcinoma with contrast-enhanced sonography using intermittent harmonic imaging. *Cancer* 2005; 104:2373-2383.
28. Konig K, Scheipers U, Pesavento A, Lorenz A, Ermert H, Senge T. Initial experiences with real-time elastography guided biopsies of the prostate. *J Urol* 2005; 174:115-117.
29. Frauscher F, Klauser A, Koppelstaetter F, Mallouhi A, Horninger W, Zur ND. Real-time elastography for prostate cancer detection: Preliminary experience. *Eur Radiol* 2004; 14:150.
30. Prando A, Wallace S. Helical CT of prostate cancer: early clinical experience. *AJR Am J Roentgenol.* 2000; 175:343-346.
31. Beyersdorff D, Taupitz M, Winkelmann B, et al. Patients with a history of elevated prostate-specific antigen levels and negative transrectal US-guided quadrant or sextant biopsy results: value of MRI. *Radiology* 2002; 224:701-706.
32. Kurhanewicz J, Vigneron DB, Hricak H, Narayan P, Carroll P, Nelson SJ. Three-dimensional H-1 MR spectroscopic imaging of the in situ human prostate with high (0.24-0.7-cm³) spatial resolution. *Radiology* 1996; 198:795-805.
33. Heerschap A, Jager GJ, Graaf M van der, et al. In vivo proton MR spectroscopy reveals altered metabolite content in malignant prostate tissue. *Anticancer Res* 1997; 17:1455-1460.

34. Scheidler J, Hricak H, Vigneron DB, et al. Prostate cancer: localization with three-dimensional proton MR spectroscopic imaging—clinicopathologic study. *Radiology* 1999; 213:473-480.
35. Fütterer JJ, Heijmink SW, Scheenen TW, et al. Prostate cancer localization with dynamic contrast-enhanced MRI and proton MR spectroscopic imaging. *Radiology*. 2006; 241:449-458.
36. Barentsz JO, Engelbrecht M, Jager GJ, et al. Fast dynamic gadolinium-enhanced MRI of urinary bladder and prostate cancer. *J Magn Reson Imaging* 1999; 10:295-304.
37. Donahue KM, Weisskoff RM, Parmelee DJ, et al. Dynamic Gd-DTPA enhanced MRI measurement of tissue cell volume fraction. *Magn Reson Med* 1995; 34:423-432.
38. Huisman HJ, Engelbrecht MR, Barentsz JO. Accurate estimation of pharmacokinetic contrast-enhanced dynamic MRI parameters of the prostate. *J Magn Reson Imaging* 2001; 13:607-614.
39. Kiessling F, Lichy M, Grobholz R, et al. Detection of prostate carcinomas with T1-weighted dynamic contrast-enhanced MRI. Value of two-compartment model. *Radiologe*. 2003; 43: 474-480.
40. Engelbrecht MR, Huisman HJ, Laheij RJ, et al. Discrimination of prostate cancer from normal peripheral zone and central gland tissue by using dynamic contrast-enhanced MRI. *Radiology* 2003; 229:248-254.
41. Van Dorsten FA, Van Der Graaf M., Engelbrecht MR, et al. Combined quantitative dynamic contrast-enhanced MRI and (1)H MR spectroscopic imaging of human prostate cancer. *J Magn Reson Imaging* 2004; 20:279-287.
42. Shreve PD, Grossman HB, Gross MD, Wahl RL. Metastatic prostate cancer: initial findings of PET with 2-deoxy-2-[F-18]fluoro-D-glucose. *Radiology* 1996; 199:751-756.
43. Effert PJ, Bares R, Handt S, Wolff JM, Bull U, Jakse G. Metabolic imaging of untreated prostate cancer by positron emission tomography with 18fluorine-labeled deoxyglucose. *J Urol* 1996; 155:994-998.
44. Haseman MK, Reed NL, Rosenthal SA. Monoclonal antibody imaging of occult prostate cancer in patients with elevated prostate-specific antigen. Positron emission tomography and biopsy correlation. *Clin Nucl Med* 1996; 21:704-713.
45. Liu JJ, Zafar MB, Lai YH, Segall GM, Terris MK. Fluorodeoxyglucose positron emission tomography studies in diagnosis and staging of clinically organ-confined prostate cancer. *Urology* 2001; 57:108-111.
46. Sutinen E, Nurmi M, Roivainen A, et al. Kinetics of [(11)C]choline uptake in prostate cancer: a PET study [correction for study]. *Eur J Nucl Med Mol Imaging* 2004; 31:317-324.
47. Ross PL, Scardino PT, Kattan MW. A catalog of prostate cancer nomograms. *J Urol* 2001; 165:1562-1568.
48. Ross PL, Gerigk C, Gonen M, et al. Comparisons of nomograms and urologists' predictions in prostate cancer. *Semin Urol Oncol* 2002; 20:82-88.
49. Reckwitz T, Potter SR, Partin AW. Prediction of locoregional extension and metastatic disease in prostate cancer: a review. *World J Urol* 2000; 18:165-172.
50. Khan MA, Partin AW. Partin tables: past and present. *BJU Int* 2003; 92:7-11.
51. Sobin LH, Wittekind CH. UICC: TNM Classification of Malignant Tumors, 6th edn Wiley-Liss, New York, 2002.
52. Heiken JP, Forman HP, Brown JJ. Neoplasms of the bladder, prostate and testis. *Radiol Clin North Am* 1994; 32:81-98.
53. Fütterer JJ, Engelbrecht MR, Jager GJ, et al. Prostate cancer: comparison of local staging accuracy of pelvic phased-array coil alone versus integrated endorectal-pelvic phased-array coils. Local staging accuracy of prostate cancer using endorectal coil MRI. *Eur Radiol*. 2007; 17:1055-1065.
54. May F, Treumann T, Dettmar P, et al. Limited value of endorectal magnetic resonance imaging and transrectal ultrasonography in the staging of clinically localized prostate cancer. *BJU int* 2001; 87:66-69.
55. Sauvain JL, Palasack P, Bourscheid D, et al. Value of power Doppler and 3D vascular sonography as a method for diagnosis and staging of prostate cancer. *Eur Urol* 2003; 44:21-31.

56. Presti JC, Jr., Hricak H, Narayan PA, Shinohara K, White S, Carroll PR. Local staging of prostatic carcinoma: comparison of transrectal sonography and endorectal MRI. *AJR Am J Roentgenol* 1996; 166:103-108.
57. Ekici S, Ozen H, Agildere M, et al. A comparison of transrectal ultrasonography and endorectal magnetic resonance imaging in the local staging of prostatic carcinoma. *BJU Int* 1999; 83:796-800.
58. Garg S, Fortling B, Chadwick D, Robinson MC, Hamdy FC. Staging of prostate cancer using 3-dimensional transrectal ultrasound images: a pilot study. *J Urol* 1999; 162:1318-1321.
59. Okihara K, Kamoi K, Lane RB, Evans RB, Troncoco P, Babaian RJ. Role of systematic ultrasound-guided staging biopsies in predicting extraprostatic extension and seminal vesicle invasion in men with prostate cancer. *J Clin Ultrasound* 2002; 30:123-131.
60. Burcombe RJ, Ostler PJ, Ayoub AW, Hoskin PJ. The role of staging CT scans in the treatment of prostate cancer: a retrospective audit. *Clin Oncol (R Coll Radiol)* 2000; 12:32-35.
61. Huncharek M, Muscat J. Serum prostate-specific antigen as a predictor of staging abdominal/pelvic computed tomography in newly diagnosed prostate cancer. *Abdom Imaging*. 1996; 21:364-367.
62. Tarcan T, Turkeri L, Biren T, Kullu S, Gurmen N, Akdas A. The effectiveness of imaging modalities in clinical staging of localized prostatic carcinoma. *Int Urol Nephrol* 1996; 28:773-779.
63. Barbieri A, Monica B, Sebastio N, Incarbone GP, Di Stefano C. Value and limitations of transrectal ultrasonography and computer tomography in preoperative staging of prostate carcinoma]. *Acta Biomed Ateneo Parmense* 1997; 68:23-26.
64. Sonnad SS, Langlotz CP, Schwartz JS. Accuracy of MRI for staging prostate cancer: a meta-analysis to examine the effect of technologic change. *Acad Radiol* 2001; 8:149-157.
65. Engelbrecht MR, Jager GJ, Laheij RJ, Verbeek AL, van Lier HJ, Barentsz JO. Local staging of prostate cancer using magnetic resonance imaging: a meta-analysis. *Eur Radiol* 2002; 12:2294-2302.
66. Wang L, Mullerad M, Chen HN, et al. Prostate cancer: incremental value of endorectal MRI findings for prediction of extracapsular extension. *Radiology* 2004; 232:133-139.
67. Engelbrecht MR, Jager GJ, Severens JL. Patient selection for magnetic resonance imaging of prostate cancer. *Eur Urol* 2001; 40:300-307.
68. Jager GJ, Severens JL, Thornbury JR, de la Rosette JJ, Ruijs SH, Barentsz JO. Prostate cancer staging: should MRI be used?—A decision analytic approach. *Radiology* 2000; 215:445-451.
69. Langlotz CP, Schnall MD, Malkowicz SB, Schwartz JS. Cost-effectiveness of endorectal magnetic resonance imaging for the staging of prostate cancer. *Acad Radiol* 1996; 3 Suppl 1:S24-S27.
70. Fütterer JJ, Engelbrecht MR, Huisman HJ, et al. Staging Prostate Cancer with Dynamic Contrast-enhanced Endorectal MRI prior to Radical Prostatectomy: Experienced versus Less Experienced Readers. *Radiology* 2005; 237:541-549.
71. Yu KK, Scheidler J, Hricak H, et al. Prostate cancer: prediction of extracapsular extension with endorectal MRI and three-dimensional proton MR spectroscopic imaging. *Radiology* 1999; 213:481-488.
72. Fütterer JJ, Heijmink SW, Scheenen TW, et al. Prostate cancer: local staging at 3-T endorectal MRI—early experience. *Radiology* 2006; 238:184-191.
73. Heijmink SWTPJ, Fütterer JJ, Hambrock T, et al. Body Array versus Endorectal coil MRI of Prostate Cancer at 3 Tesla: Comparison of Image Quality, Localization, and Staging Performance with Whole-Mount Section Histopathology as Standard of Reference. *Radiology* 2007; in press.
74. Lawrentschuk N, Davis ID, Bolton DM, Scott AM. Positron emission tomography and molecular imaging of the prostate: an update. *BJU Int*. 2006; 97:923-931.
75. Messing EM, Manola J, Sarosdy M, Wilding G, Crawford ED, Trump D. Immediate hormonal therapy compared with observation after radical prostatectomy and pelvic lymphadenectomy in men with node-positive prostate cancer. *N Engl J Med* 1999; 341(24):1781-1788.
76. Walsh PC. Surgery and the reduction of mortality from prostate cancer. *N Engl J Med* 2002; 347(11):839-840.

77. Magnusson A, Fritjofsson A, Norlen BJ, Wicklund H. The value of computed tomography and ultrasound in assessment of pelvic lymph node metastases in patients with clinically locally confined carcinoma of the prostate. *Scand J Urol Nephrol* 1988; 22:7-10.
78. Flanigan RC, McKay TC, Olson M, Shankey TV, Pyle J, Waters WB. Limited efficacy of preoperative computed tomographic scanning for the evaluation of lymph node metastasis in patients before radical prostatectomy. *Urology* 1996; 48:428-432.
79. Borley N, Fabrin K, Sriprasad S, et al. Laparoscopic pelvic lymph node dissection allows significantly more accurate staging in "high-risk" prostate cancer compared to MRI or CT. *Scand J Urol Nephrol* 2003; 37:382-386.
80. Jager GJ, Barentsz JO, Oosterhof GO, Witjes JA, Ruijs SJ. Pelvic adenopathy in prostatic and urinary bladder carcinoma: MRI with a three-dimensional T1-weighted magnetization-prepared-rapid gradient-echo sequence. *AJR Am J Roentgenol* 1996; 167:1503-1507.
81. Harisinghani MG, Barentsz J, Hahn PF, et al. Noninvasive detection of clinically occult lymph-node metastases in prostate cancer. *N Engl J Med* 2003; 348:2491-2499.
82. Weissleder R, Elizondo G, Wittenberg J, et al. Ultrasmall paramagnetic iron oxide: an intravenous contrast agent for assessing lymph nodes with MRI. *Radiology* 1990; 175:494-498.
83. Vassallo P, Matei C, Heston WDW, et al. AMI-227-enhanced MR Lymphography: usefulness for differentiating reactive from tumor-bearing lymph nodes. *Radiology* 1994; 193:501-506.
84. Heesakkers RA, Fütterer JJ, Hovels AM, et al. Prostate cancer evaluated with ferumoxtran-10-enhanced T2*-weighted MRI at 1.5 and 3.0 T: early experience. *Radiology* 2006; 239:481-487.
85. Heicappell R, Muller-Mattheis V, Reinhardt M, et al. Staging of pelvic lymph nodes in neoplasms of the bladder and prostate by positron emission tomography with 2-[(18)F]-2-deoxy-D-glucose. *Eur Urol* 1999; 36:582-587.
86. Lentle BC, McGowan DG, Dierich H. Technetium-99M polyphosphate bone scanning in carcinoma of the prostate. *Br J Urol* 1974; 46:543-548.
87. Elkin M, Mueller HP. Metastases from cancer of the prostate; autopsy and roentgenological findings. *Cancer* 1954; 7:1246-1248.
88. Abuzalouf S, Dayes I, Lukka H. Baseline staging of newly diagnosed prostate cancer: a summary of the literature. *J Urol* 2004; 171:2122-2127.
89. Oesterling JE, Martin SK, Bergstralh EJ, Lowe FC. The use of prostate-specific antigen in staging patients with newly diagnosed prostate cancer. *JAMA* 1993; 269:57-60.
90. Lauenstein TC, Goehde SC, Herborn CU, et al. Whole-body MRI: evaluation of patients for metastases. *Radiology* 2004; 233:139-148.
91. Shreve PD, Grossman HB, Gross MD, Wahl RL. Metastatic prostate cancer: initial findings of PET with 2-deoxy-2-[F-18]fluoro-D-glucose. *Radiology* 1996; 199:751-756.
92. Garner MJ, Turner MC, Ghadirian P, Krewski D. Epidemiology of testicular cancer: an overview. *Int J Cancer*. 2005;116(3):331-339.
93. Comiter CV, Benson CJ, Capelouto CC, et al: Nonpalpable intratesticular masses detected sonographically. *J Urol* 1995; 154:1367-1369.
94. National Cancer Institute. SEER Cancer Statistics Review, 1975-2001. Bethesda, MD, 2004. Available at: http://seer.cancer.gov/csr/1975_2001/. Accessed June 15, 2006.
95. Dalal PU, Sohaib SA, Huddart R. Imaging of testicular germ cell tumors. *Cancer Imaging* 2006; 6:124-134.
96. Coakley FV, Hricak H, Presti JC Jr. Imaging and management of atypical testicular masses. *Urol Clin North Am* 1998; 25:375-388.
97. Hernes EH, Harstad K, Fossa SD. Changing incidence and delay of testicular cancer in southern Norway (1981-1992). *Eur Urol* 1996; 30:349-357.
98. Hricak H. Imaging of the scrotum. Textbook and atlas, New York, Raven press, 1995:49-93.
99. Guthrie JA, Fowler RC. Ultrasound diagnosis of testicular tumors presenting as epididymal disease. *Clin Radiol* 1992; 46: 397-400.
100. Grantham JG, Charboneau JW, James EM, et al. Testicular neoplasms: 29 tumors studied by high-resolution US. *Radiology* 1985; 157: 775-780.
101. Senay BA, Stein BS. Testicular neoplasm diagnosed by ultrasound. *J Surg Oncol* 1986; 32: 110-112

102. Rifkin MD, Kurtz AB, Pasto ME, Goldberg BB. Diagnostic capabilities of high-resolution scrotal ultrasonography: prospective evaluation. *J Ultrasound Med* 1985; 4:13-19.
103. Oyen R. Imaging of testicular neoplasms. In: *Carcinoma of the kidney and testis, and rare malignancies. Innovations in management.* Springer Verlag, 1999;203-210.
104. Schwerk WB, Schwerk WN, Rodeck G: Testicular tumors: Prospective analysis of real-time US patterns and abdominal staging. *Radiology* 1987; 164:369-374.
105. Benson CB, Doubilet PM, Richie JP: Sonography of the male genital tract. *Am J Roentgenol* 1989; 153:705-713.
106. Ciftci AO, Bingol-Kologlu M, Senocak ME, et al. Testicular tumors in children. *J Pediatr Surg* 2001; 36:1796-1801.
107. Backus ML, Mack LA, Middleton WD, King BF, Winter TC, True LD. Testicular micro-lithiasis: imaging appearances and pathologic correlation. *Radiology* 1994; 192:781-785.
108. Peckham MJ, Barrett A, McEwain TJ, Hendry WF, Raghaven D. Non-seminoma germ cell tumors (malignant teratomas) of the testis. *BJU* 1981; 53:162-172.
109. Donohue JP, Zachary JM, Maynard BR. Distribution of nodal metastases in nonseminomatous testis cancer. *J Urol* 1982; 128:315-320.
110. Mason MD, Featherstone T, Olliff J, Horwich A. Inguinal and iliac lymph node involvement in germ cell tumors of the testis: implications for radiological investigation and for therapy. *Clin Oncol* 1991; 3:147-150.
111. Siegel MJ: The acute scrotum. *Radiol Clin North Am* 1997; 35:959-976.
112. Horstman WG, Melson GL, Middleton WD, Andriole GL. Testicular tumors: findings with color Doppler US. *Radiology* 1992; 185:733-737.
113. Kundra V. Testicular cancer. *Semin Roentgenol* 2004; 39:437-450.
114. Watanabe Y, Dohke M, Ohkubo K, et al. Scrotal disorders: evaluation of testicular enhancement patterns at dynamic contrast-enhanced subtraction MRI. *Radiology* 2000; 217:219-227.
115. Schultz-Lampel D, Bogaert G, Thuroff JW, Schlegel E, Cramer B. MRI for evaluation of scrotal pathology. *Urol Res* 1991; 19:289-292.
116. Cramer BM, Schlegel EA, Thuroff JW. MRI in the differential diagnosis of scrotal and testicular disease. *Radiographics.* 1991; 11:9-21.
117. Albers P, Bender H, Yilmaz H, Schoeneich G, Biersack HJ, Mueller SC. Positron emission tomography in the clinical staging of patients with Stage I and II testicular germ cell tumors. *Urology.* 1999; 53:808-811.
118. Muller-Mattheis V, Reinhardt M, Gerharz CD, et al. Positron emission tomography with [18 F]-2-fluoro-2-deoxy-D-glucose (18FDG-PET) in diagnosis of retroperitoneal lymph node metastases of testicular tumors. *Urologe A.* 1998; 37:609-620.
119. Spermon JR, De Geus-Oei LF, Kiemeny LA, Witjes JA, Oyen WJ. The role of (18)fluoro-2-deoxyglucose positron emission tomography in initial staging and re-staging after chemotherapy for testicular germ cell tumors. *BJU Int.* 2002; 89:549-556.
120. Gambhir SS, Czernin J, Schwimmer J, et al. A tabulated summary of the FDG PET literature. *J Nucl Med* 2001; 42:1S-93S
121. De Santis M, Becherer A, Bokemeyer C, et al. 2-18fluoro-deoxy-D-glucose positron emission tomography is a reliable predictor for viable tumor in postchemotherapy seminoma: an update of the prospective multicentric SEMPET trial. *J Clin Oncol.* 2004;22(6):1034-1039.
122. Donohue JP, Thornhill JA, Foster RS, Rowland RG, Bihrl R. Primary retroperitoneal lymph node dissection in clinical stage A non-seminomatous germ cell testis cancer. Review of the Indiana University experience 1965-1989. *Br J Urol.* 1993; 71:326-335.
123. Hilton S, Herr HW, Teitcher JB, Begg CB, Castellino RA. CT detection of retroperitoneal lymph node metastases in patients with clinical stage I testicular nonseminomatous germ cell cancer: assessment of size and distribution criteria. *AJR Am J Roentgenol.* 1997; 169: 521-525.
124. Fernandez EB, Moul JW, Foley JP, Colon E, McLeod DG. Retroperitoneal imaging with third and fourth generation computed axial tomography in clinical stage I nonseminomatous germ cell tumors. *Urology* 1994; 44:548-552.

125. See W.A., Hoxie L. Chest staging in testis cancer patients: imaging modality selection based upon risk assessment as determined by abdominal computerized tomography scan results. *J Urol* 1993; 150:874-878.
126. Ellis JH, Bies JR, Kopeccky KK, Klatte EC, Rowland RG, Donohue JP. Comparison of NMR and CT imaging in the evaluation of metastatic retroperitoneal lymphadenopathy from testicular carcinoma. *J Comput Assist Tomogr.* 1984; 8:709-719.
127. Hogeboom WR, Hoekstra HJ, Mooyaart, EL et al. The role of magnetic resonance imaging and computed tomography in the treatment evaluation of retroperitoneal lymph-node metastases of non-seminomatous testicular tumors. *Eur J Radiol.* 1991; 13:31-36.
128. Harisinghani MG, Saksena M, Ross RW, Tabatabaei S, A pilot study of lymphotrophic nanoparticle-enhanced magnetic resonance imaging technique in early stage testicular cancer: a new method for non-invasive lymph node evaluation. *Urology.* 2005; 66:1066-1071.
129. Satoh M, Ito A, Kaiho Y, et al. Intraoperative, radio-guided sentinel lymph node mapping in laparoscopic lymph node dissection for Stage I testicular carcinoma. *Cancer.* 2005; 103:2067-2072.
130. P Warde, MK Gospodarowicz, T Panzarella, CN Catton Stage I testicular seminoma: results of adjuvant irradiation and surveillance. *J Clin Oncol.* 1995; 13:2255-2262.
131. Cremerius U, Wildberger JE, Borchers H, et al. Does positron emission tomography using 18-fluoro-2-deoxyglucose improve clinical staging of testicular cancer?—Results of a study in 50 patients. *Urology* 1999; 54:900-904.
132. Hain SF, O'Doherty MJ, Timothy AR, et al. Fluorodeoxyglucose PET in the initial staging of germ cell tumors. *Eur J Nucl Med* 2000; 27:590-594.
133. Flechon A, Bompas E, Biron P, Droz JP. Management of post-chemotherapy residual masses in advanced seminoma. *J Urol* 2002; 168:1975-1979.
134. Steyerberg EW, Gerl A, Fossa SD, et al. Validity of predictions of residual retroperitoneal mass histology in nonseminomatous testicular cancer. *J Clin Oncol* 1998; 16:269-274.
135. Rustin GJ, Mead GM, Stenning SP, et al. National Cancer Research Institute Testis Cancer Clinical Studies Group. Randomized trial of two or five computed tomography scans in the surveillance of patients with stage I nonseminomatous germ cell tumors of the testis: Medical Research Council Trial TE08, ISRCTN56475197—the National Cancer Research Institute Testis Cancer Clinical Studies Group. *J Clin Oncol* 2007; 25:1310-1315.
136. Albers P, Albrecht W, Algaba F, Bokemeyer C, Cohn-Cedermark G, Horwich A, Klepp O, Laguna MP, Pizzocaro G. Guidelines on testicular cancer. *Eur Urol* 2005; 48:885-894.